

We are IntechOpen, the world's leading publisher of Open Access books Built by scientists, for scientists

6,900

Open access books available

186,000

International authors and editors

200M

Downloads

Our authors are among the

154

Countries delivered to

TOP 1%

most cited scientists

12.2%

Contributors from top 500 universities



WEB OF SCIENCE™

Selection of our books indexed in the Book Citation Index
in Web of Science™ Core Collection (BKCI)

Interested in publishing with us?
Contact book.department@intechopen.com

Numbers displayed above are based on latest data collected.
For more information visit www.intechopen.com



Evaluation of the Shielding Gas Influence on the Weldability of Ferritic Stainless Steel

Demostenes Ferreira Filho¹, Ruham Pablo Reis¹
and Valtair Antonio Ferraresi²

¹Federal University of Rio Grande/School of Engineering

²Federal University of Uberlândia/Faculty of Mechanical Engineering
Brazil

1. Introduction

The use of stainless steels has been nowadays widespread in a number of industrial sectors. They usually offer exceptional performance regarding mechanical and corrosion properties, but according to Lee et al. (2008) stainless steels are considered as high cost materials as far as solutions for structural engineering are concerned. However, this material group can provide aesthetic characteristics as well as outstanding versatility, easy cleaning and maintenance conditions. Nevertheless, there are still plentiful possibilities for applying stainless steels in new situations or improving their use in current applications due to their appealing visual aspect and durability.

In the automotive industry, for instance, parts of the exhaust system are in general composed of tubes and blanks (stamped metal sheets) that usually are welded and have ferritic stainless steels as the main base material. According to Alves et al. (2002), the main ferritic stainless steels used in the hot portion of automotive exhaust systems are the AISI 409 and 441. On the other hand, in the cold portion the AISI 409, 439 and 436 are normally utilized.

Faria (2006) states that automotive exhaust systems went through a number of changes along the last 20 years as a consequence of more restrict pollution policies, needs for longer durability and higher engine efficiencies as well as requirements for reduction in weight and costs. Stainless steels used in the hot parts of automotive exhaust systems, according to Sekita et al. (2004), must be refractory, which can be accomplished by niobium additions, high levels of molybdenum and optimized silicon presence. The same authors also mention the importance of having a good formability in such hot parts.

The market for stainless steels has experienced constant growth because of their excellent properties and continuous improvement in manufacturing of these materials, especially when issues like increase in process productivity and reduction in costs are taken into consideration. However, recently there has been a sharp increase in the international prices of alloying elements largely used in stainless steels, mainly nickel and molybdenum. As a result, the most traditional stainless steels class (austenitic) went through severe price rise worldwide. Fortunately, the ferritic class, which contains no nickel, emerges as an alternative for some applications, but sometimes some drawbacks have to be figured out before replacing the austenitic class.

One of the main problems found in certain ferritic stainless steels applications is related to their weldability, but, according to Schwarz & Tessin (2003), advantages concerning fatigue strength and general corrosion behavior can be achieved with ferritic filler materials. According to Reddy & Mohandas (2001), ferritic class base materials welded with ferritic wires exhibit greater resistance to stress corrosion cracking when compared with weldments produced with austenitic wires. However, grain coarsening in the fusion zone often takes place. Renaudot et al. (2000) state that the welding of ferritic stainless steels with filler metals also made of ferritic stainless steels minimizes the metallurgical discontinuity around the weld bead and promotes better metallurgical compatibility between the base metal and molten zone due to small differences in microstructure and thermal dilatation. The same authors point out that a ferritic class, namely the ER409Nb, filler metal has been utilized since the 90's for welding low-chromium ferritic stainless steels. Tests carried out with this wire resulted in welds with good geometry quality, ductility and resistance to intergranular corrosion. This result is also cited by Inui et al. (2003). These authors also mention that the weld metal of ferritic stainless steels has a large columnar structure, often leading to a decrease in cracking resistance and high temperature strength. Furthermore, they also reported that large grains deteriorate oxidation resistance and corrosion resistance of the weld metal. Balmforth & Lippold (2000), mention that the mechanical properties of the weld zone of ferritic stainless steels are very sensitive to the microstructure constituents, and poor microstructure control, like martensite presence in the fusion zone, can limit their application.

Ferritic wires might contain different elements in their chemical composition such as Titanium, Niobium and Aluminum, as a way of improving mechanical properties and resistance to corrosion of the welded joints. Considering thus the variability of ferritic wires available, Inui et al. (2003) tested three types of non-commercial filler metals made of stabilized ferritic stainless steels to weld plates also made of ferritic stainless steels; one wire stabilized with titanium, one stabilized with niobium and aluminum and another one with niobium, titanium and aluminum. The authors verified that the presence of Aluminum, titanium and niobium in adequate fractions was able to produce fusion zones with fine grains and, therefore, better mechanical properties.

Madeira & Modenesi (2007), claim that the addition of niobium and/or titanium, and the consequent stabilization, can reduce the formation of martensite, maintaining a ferritic structure, and decrease the grain growth in the fusion zone. Wang & Wang (2008), cited, that Titanium carbonitrates have high thermal stability during welding, especially after high heat inputs. Another important fact is that with the stabilization of ferritic stainless steel wires there is also an inhibition in the formation of chromium carbides and nitrates, which are directly related to intergranular corrosion in welded structures. The main stabilizing elements are niobium and titanium. Madeira (2007) compared the results of the ER430Ti and ER430LNb wires using Ar+2%O₂ as shielding gas in GMA welding. A higher penetration in the weld beads was observed when the ER430Ti was used. This took place for the same welding setting (voltage and wire feed rate) in the power source, but higher current levels were needed for the same fusion rate compared to the other wire. It was concluded that the increase in penetration is related to the higher electrical resistivity of the ER430Ti wire in relation to that one found in the ER430LNb wire. Electrical resistivity values were measured by Resende (2007) in a comparative manner for the ER308LSi, ER430Ti and ER430LNb filler metals. He noticed that the first two wires had relatively similar resistivity values whilst the third one had a lower level. From the same reference, a comparison was carried out

regarding the weld beads produced with the ER430Ti and ER430LNb wires. The weld bead appearance resulted from the ER430Ti utilization was significantly inferior (lower wettability and poor superficial quality). This fact was mainly linked to the ER430Ti superficial roughness, which resulted in an irregular feeding. In spite of the references presented so far, there is still lack of information concerning the weldability of ferritic stainless steels.

Concerning the welding of the ferritic stainless steels, Stenbacka & Persson (1992) mention that GMA welding of stainless steels is commonly carried out shielded by argon with low levels of an oxidant (O_2 or CO_2). According to them, the presence of oxidizing components blended with argon promotes arc stability and metal transfer improvement. The advantage of the CO_2 addition in the shielding gas mixture would be cost reduction related, yet metal transfer is strongly affected. The same authors believe that a small amount of CO_2 added to argon should be used for short-circuiting transfer. According to Chae et al. (2008), the addition of CO_2 to argon improves the wettability of the weld bead, improving the weld quality. However, Strassburg (1976) claims that an increase in the proportion of oxidizing elements in the shielding gas increases the loss of molybdenum, chromium and niobium. Lundvist (1980), states that the addition of CO_2 in the shielding gas result in carbon absorption and also in oxidation of the deposited metal. The negative aspect related to carbon incorporation into the weld pool is that the content of ferrite in the weld bead might get lower; as carbon is a strong austenite producer at high temperatures, during cooling, martensite might form along the ferritic grain boundaries, impairing the tenacity of the welded joint.

There have been some studies about the shielding gas used for welding austenitic stainless steels. Tusek & Suban (2000), for instance, studied the effect of hydrogen in argon as the shielding gas for arc welding of this stainless steel class. When GMA welding was used, the hydrogen addition to argon increases melting rate and melting efficiency of the arc, but the increase is much smaller than in GTA welding. Durgutlu (2004) reported the effect of hydrogen added to argon during GTA welding of 316L austenitic stainless steel plates. In this case, the mean grain size in the weld bead increased with rising hydrogen contents. In addition, the weld bead penetration depth and width increased as the hydrogen content was raised. Gülenç et al. (2005) studied GMA welding of 304L stainless steel samples and observed that the toughness of the weld beads increases with rising Hydrogen amount added to argon and with increase in the welding current level. Liao & Chen (1998) examined how the microstructure and mechanical properties of 304 stainless steel welds are influenced by mixtures of carbon dioxide (2 to 20%) in argon. They detected that spattering increases, notch toughness is affected by the delta-ferrite amount and oxidation potential, specially at room temperature with increase in the CO_2 content.

Despite the facts discussed so far, the volume of information available in the current literature about GMA welding with ferritic stainless steels wires is still very scarce, mainly in relation to the shielding gas effect on the welded joints. Thus, this manuscript aims to analyze the metallurgical characteristics of a ferritic stainless steel weldments by studying the influence of the shielding gas (argon by itself and blended with O_2 or CO_2) on the chemical composition, microstructure, hardness and ductility of the weld beads. It is expected that a broader insight of the subject can help users and developers in the pursuit of more productive and safe welded structures (optimized filler metal and gas selection).

2. Materials and experimental procedure

In this study two different types of wires for GMA welding, namely ER430Ti and ER430LNb (both with a diameter of 1.0 mm), were used to assess the influence of stabilizing elements on the weld bead microstructure produced. The chemical composition of each wire is shown in Table 1. Each wire was combined with different shielding gases to evaluate any influence of the arc atmosphere on the weld bead chemical composition. The welded samples consisted of beads deposited side by side and in layers on the surface of 6-mm-thick plates previously cut in 40x40 mm from a UNS 43932 bi-stabilized ferritic stainless steel. The chemical composition of the base metal is presented in Table 2. This ferritic stainless steel is usually applied in automotive plants.

Wire	C	Cr	Mn	Mo	Nb	Ni	Si	Ti
ER430Ti	0.108	17.45	0.65	0.036	-	0.4	1.04	0.35
ER430LNb	0.027	17.66	0.425	0.034	0.44	0.215	0.43	0.004

Table 1. Chemical composition of the wires (weight, %).

Element	C	Cr	Mn	N	Nb	Ni	Si	V	Ti
Weight %	0.010	17.128	0.143	0.008	0.201	0.178	0.403	0.051	0.198

Table 2. Chemical composition of the UNS43932 ferritic stainless steel (weight, %).

The effectiveness of metal transfer from the wire to the weld pool and so the influence of the wire on the weld bead microstructure are mainly governed by the wire and shielding gas chemical compositions and by the type and stability of the metal transfer. The microstructure, and consequent properties, of the resultant weld bead also depend on the volume of the weld pool and on the heat input produced, which in turn will govern the thermal cycle (weld zone cooling rate from the fusion temperature). Thus, in order to have a fair comparison of welding conditions under different wire and shielding gas combinations, first of all it is necessary to find welding settings as similar as possible to each other for all the experiments. These settings are not usually the same, since the optimized situation is different for each combination of wire and shielding gas used and their pursuit is typically a complicated task due to the quantity of variables involved in GMA welding.

Thus, to have such similar welding conditions, some approaches were applied to the experiments. In order that the same metal transfer mode was achieved for all the situations, in this case the short-circuit one, the arc was kept short by using a constant voltage power supply and by setting the arc voltage always at 20 V.

The welding current is probably the most important parameter that controls heat in the arc and its delivery to the weld pool. Consequently, the current level should be virtually the same for all the samples. This intent was accomplished by appropriately setting the wire feed speed and varying the contact tip-to-work piece distance between 12 and 18 mm. The welding current accepted range was 170 ± 2 A. The WFS values set for both ER430Ti and ER430LNb wires was 7.6 m/min. As a way to reach approximately the same weld pool volume and the same heat input for all the samples, the deposition rates, for a given current level, were managed to be equivalent. This was possible by making the ratio between the

wire feed speeds and the welding travel speeds constant throughout the tests. The welding travel speed was set at 20 cm/min. Filho et al. (2010) and Ferreira Filho and Ferraresi (2008, 2010) show in details that the welding conditions and the weld bead shapes were quite similar for all the situations evaluated. The equivalency in welding conditions and weld bead shapes is crucial to avoid influence on the metallurgical formations other than that one exerted by the wire and shielding gas combination. More straightforward approaches for the experimental procedure, like just setting the same welding parameters for each combination of gas and wire, would be unfair and also lead to misjudgments.

With the welding conditions already defined, welding samples, for each combination of wire and shielding gas, were finally produced with four layers of weld beads. The characterization of the deposited molten wire in each welded sample was carried out in the central part of the cross section taken from the last weld bead of the last deposited layer. Chemical analysis of the deposits was carried out with a Solaris CCD optical emission spectrometer (one measurement for each specimen). The resultant microstructures were characterized by using a Leica DMRXP optical microscope (cross sections etched by Vilella's reagent). Samples consisted of 2-mm-thick sheets previously cut in 50x100 mm from a UNS 43932 bi-stabilized ferritic stainless steel were square butt welded with a 3 mm gap in addition as an approach to assess a situation commonly found in automotive exhaust systems. These complementary samples allowed taking into account the effect of weld bead dilution on the resultant microstructures and mechanical properties for the different shielding gas and wire combinations evaluated.

3. Results and discussions

3.1 Weld bead chemical composition

Table 3 shows the chemical composition of the weld beads produced with the different combinations of wires and shielding gases. As seen, using only argon, the weld bead composition was similar to that one of the wire in each case (Table 1).

Wire	Element	Ar	Ar+2%O ₂	Ar+2%CO ₂	Ar+4%CO ₂	Ar+8%CO ₂
ER430Ti	C	0.087	0.082	0.087	0.091	0.094
	Cr	17.391	17.489	17.444	17.515	17.500
	Mn	0.564	0.559	0.562	0.563	0.558
	Mo	0.053	0.053	0.053	0.053	0.053
	Ni	0.486	0.488	0.484	0.488	0.487
	Si	0.902	0.893	0.892	0.878	0.875
	Ti	0.323	0.305	0.298	0.273	0.247
ER430LNb	C	0.018	0.017	0.027	0.038	0.046
	Cr	18.09	18.058	18.144	18.035	18.042
	Mn	0.362	0.351	0.357	0.340	0.337
	Mo	0.050	0.049	0.050	0.049	0.049
	Nb	0.469	0.463	0.464	0.455	0.451
	Ni	0.253	0.252	0.250	0.251	0.252
	Ti	0.009	0.010	0.010	0.010	0.010

Table 3. Chemical compositions of the weld beads (weight, %).

This was expected to happen considering the fact that argon is an inert gas and the small difference found is probably related to sampling and measurement intrinsic errors. On the other hand, perceptible differences in the content of carbon, silicon, manganese, titanium and niobium took place when O_2 or CO_2 were present in the shielding gas.

Figures 1 and 2 graphically shows the changes in the percentage of carbon in the metal deposit according to the shielding gas used respectively to ER430Ti and ER430LNb. It can be noticed that with the increase in the CO_2 gas content there was a proportional increase in carbon in the weld bead, fact also observed by Lundvist (1980) and by Liao & Chen (1998). It is worth noting that with the ER430LNb wire the carbon presence was significantly larger (0.094% for 8% of CO_2 content, for instance). The ER430Ti wire led to a much lower value (0.046% for 8% of CO_2 content, for instance).

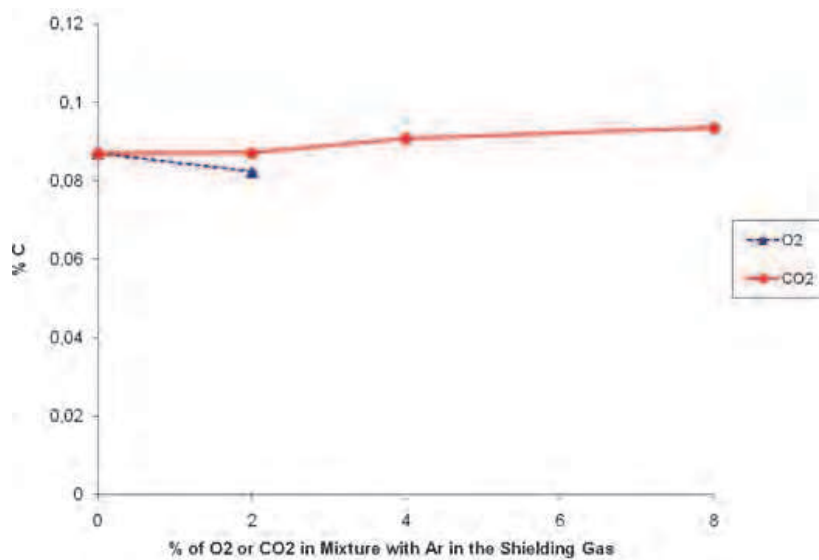


Fig. 1. Carbon presence in the weld beads versus shielding gas used for the ER430Ti wire.

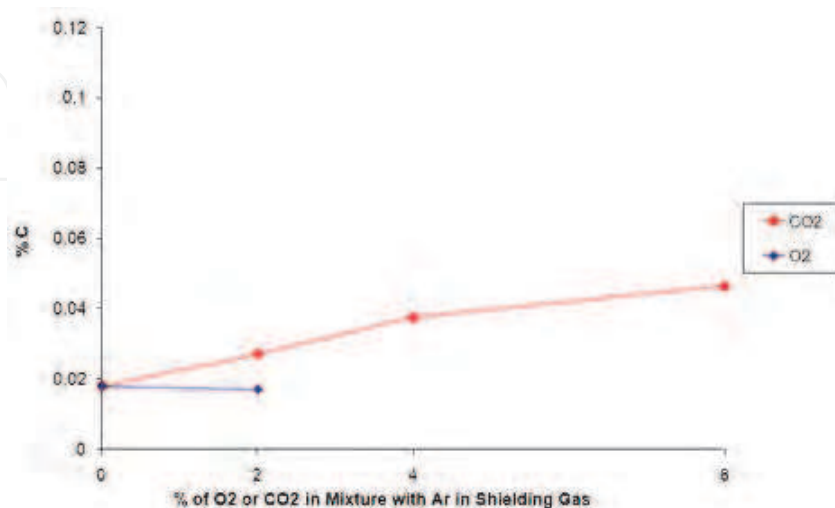


Fig. 2. Carbon presence in the weld beads versus shielding gas used for the ER430LNb wire.

Figures 3 and 4 respectively show the changes in manganese percentage in the weld bead depending on the shielding gas used to ER430Ti and ER430LNb. Figures 5 and 6 respectively show the changes in silicon percentage in the weld bead depending on the shielding gas used to ER430Ti and ER430LNb. Note that the amount of these two elements decreased in the weld beads produced with both wires as the O₂ or CO₂ content in the gas mixture was raised. This fact can be explained by the deoxidizing function of such elements. Once more the effect with the ER430Ti wire was less evident. The contents of manganese and silicon in the weld bead were much higher for the titanium alloyed wire than for the other one, which is a direct consequence of the larger presence of such elements in this wire.

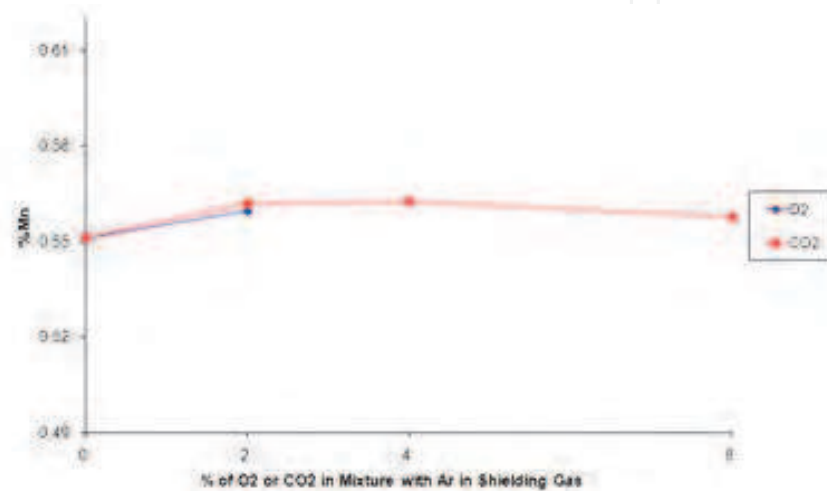


Fig. 3. Manganese presence in the weld beads versus shielding gas used for the ER430Ti wire.

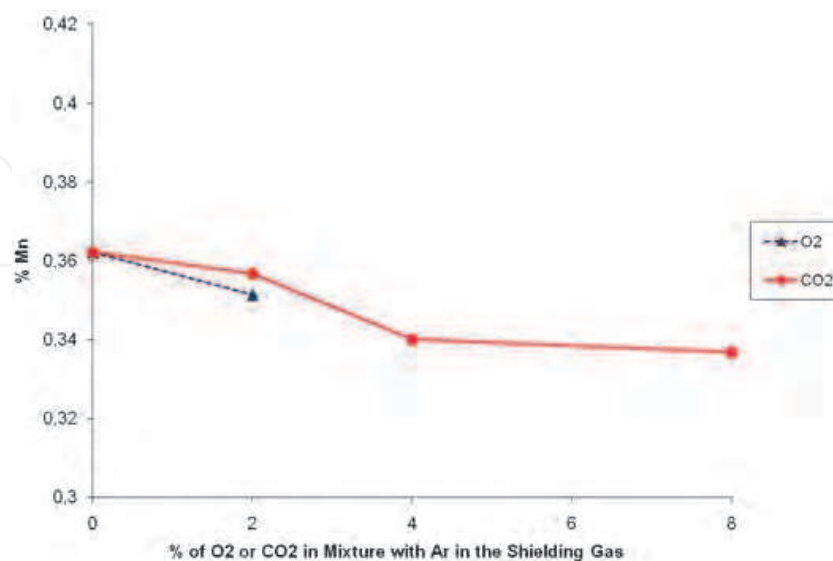


Fig. 4. Manganese presence in the weld beads versus shielding gas used for the ER430LNb wire.

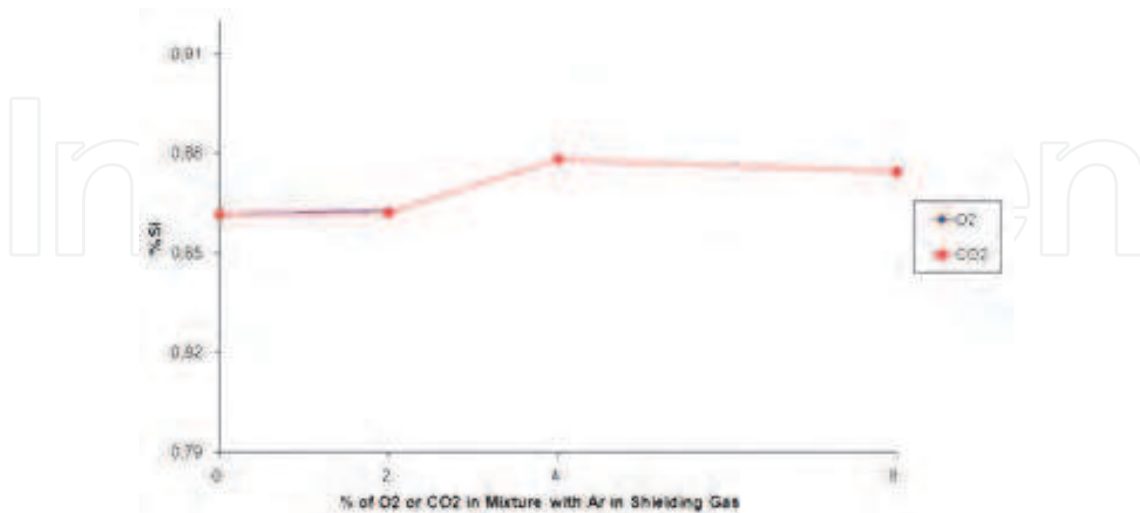


Fig. 5. Silicon presence in the weld beads versus shielding gas used for the ER430Ti wire.

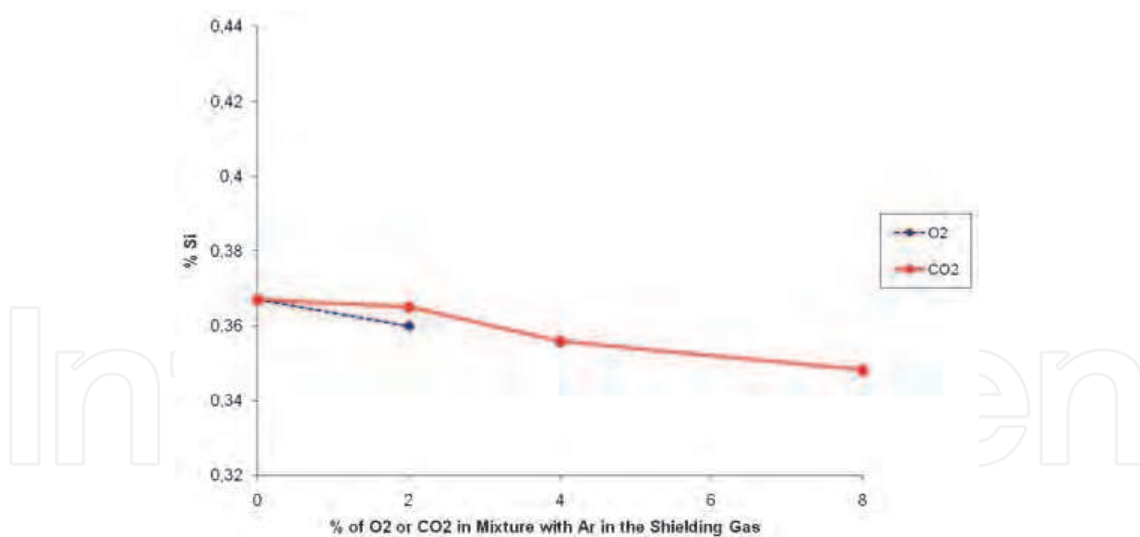


Fig. 6. Silicon presence in the weld beads versus shielding gas used for the ER430LNb wire.

Finally, Figure 7 shows the changes in the percentage of Ti in the weld bead when the ER430Ti wire was used and Figure 8 illustrates the changes in the presence of Nb in the weld bead with the use of the ER430LNb wire. The loss of Ti in the weld bead composition is more significant than the loss of Nb, especially when the weld pool is shielded by Ar+8%CO₂.

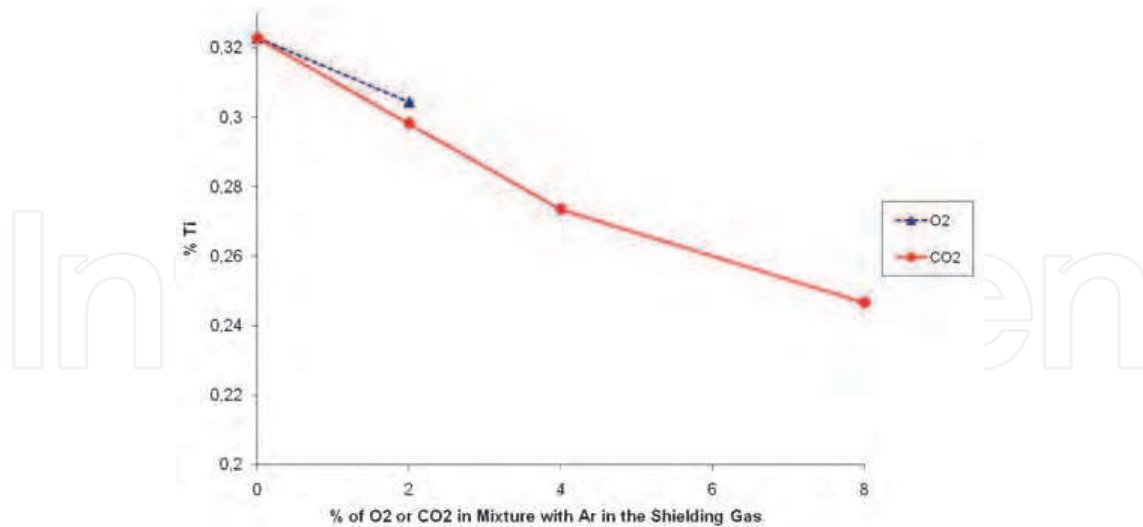


Fig. 7. Titanium presence in the weld beads versus shielding gas used for the ER430Ti wire.

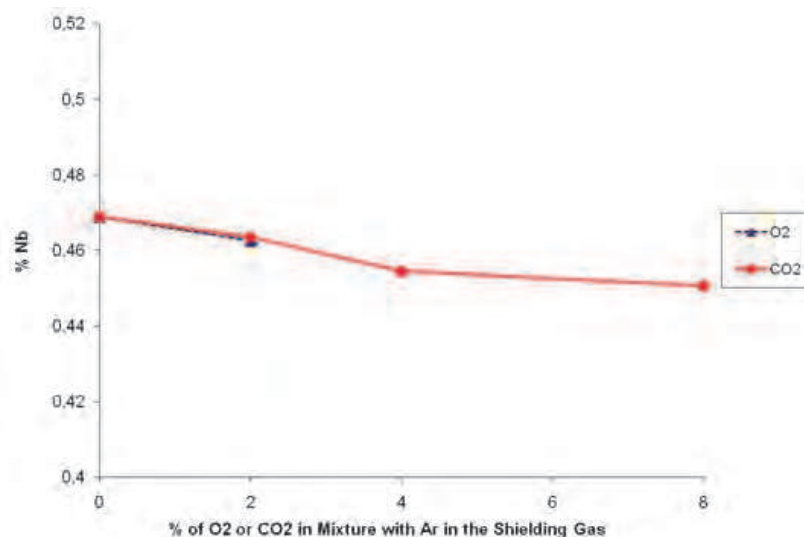


Fig. 8. Niobium presence in the weld beads versus shielding gas used for the ER430LNb wire.

3.2 Weld microstructure without dilution

Figures 9 to 13 show the microstructure of the fusion zones produced for the different combinations of wire and gas. The weld beads obtained with the ER430Ti wire (Figures 9(a) to 13(a)) contain a ferritic matrix, with columnar and coarse grains. This fact was expected, since the presence of stabilizer elements should retain grain growth as stated by Modenesi (2001). The presence of martensite and precipitates inside the grains increased as the shielding gas became more oxidizing. As seen before in Figure 1, there was an increase in carbon content in the weld pool with the presence of CO₂. This fact suggests that the severe drop in titanium amount with the increase of CO₂ contents in the shielding gas (Figure 7) is the responsible for martensite formation (it is known that titanium picks up carbon to form precipitates, retaining ferritic phases and avoiding by that martensite formation).

The microstructures of the weld beads with ER430LNb, Figures 9(b) to 13(b), were also composed of a ferritic matrix, with columnar and coarse grains. However, no presence of martensite is observed, regardless of the content of CO₂ in the shielding gas. This might be explained, despite the carbon absorption when CO₂ was used (Figure 2), by a lower content of carbon in the wire. Even so, the grains were as coarse as those found with ER430Ti wire. This fact can be explained by the Titanium precipitates high thermal stability during welding, especially after high heat inputs, as verified by Wang & Wang (2008). Niobium does not present the same grain growth effect as titanium does. It was not possible to observe changes in the precipitate quantities as the shielding gas was varied.

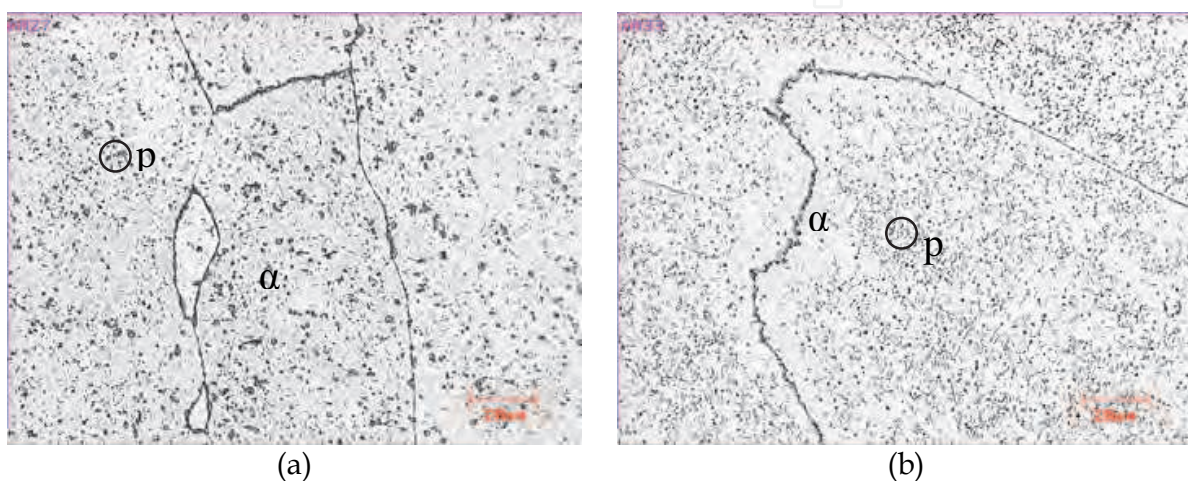


Fig. 9. Fusion zone microstructure with argon as shielding gas for the ER430Ti wire (a) and for the ER430LNb wire (b) ("α" represents ferritic matrix and "p" precipitates).

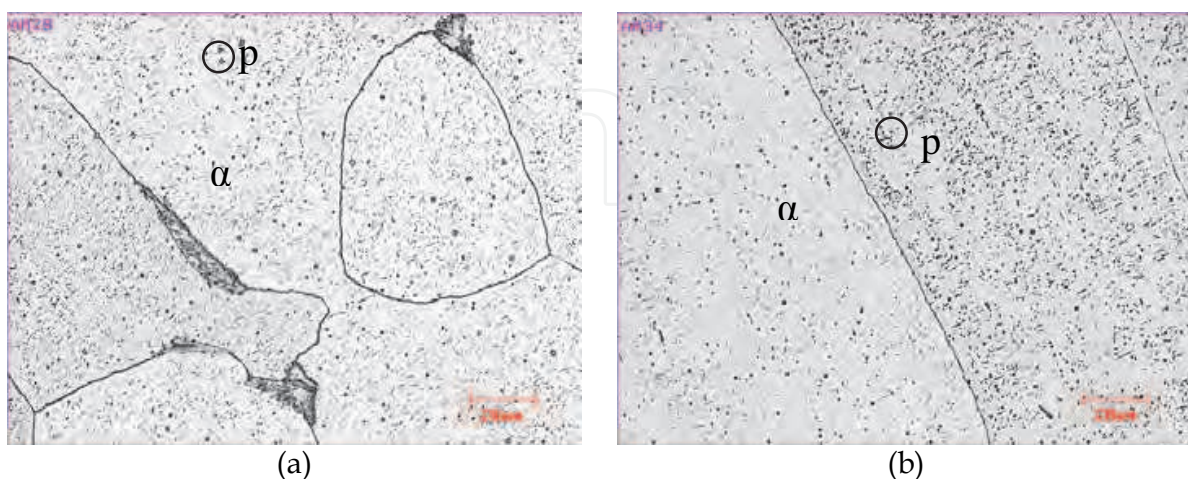


Fig. 10. Fusion zone microstructure with Ar+2%O₂ as shielding gas for the ER430Ti wire (a) and for the ER430LNb wire (b) ("α" represents ferritic matrix and "p" precipitates).

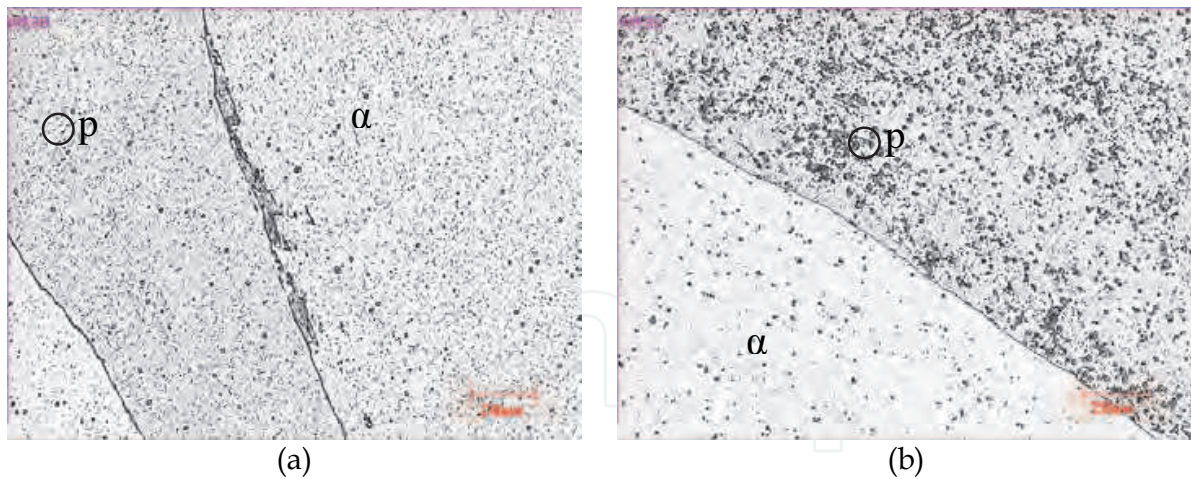


Fig. 11. Fusion zone microstructure with Ar+2%CO₂ as shielding gas for the ER430Ti wire (a) and for the ER430LNb wire (b) (" α " represents ferritic matrix and "p" precipitates).

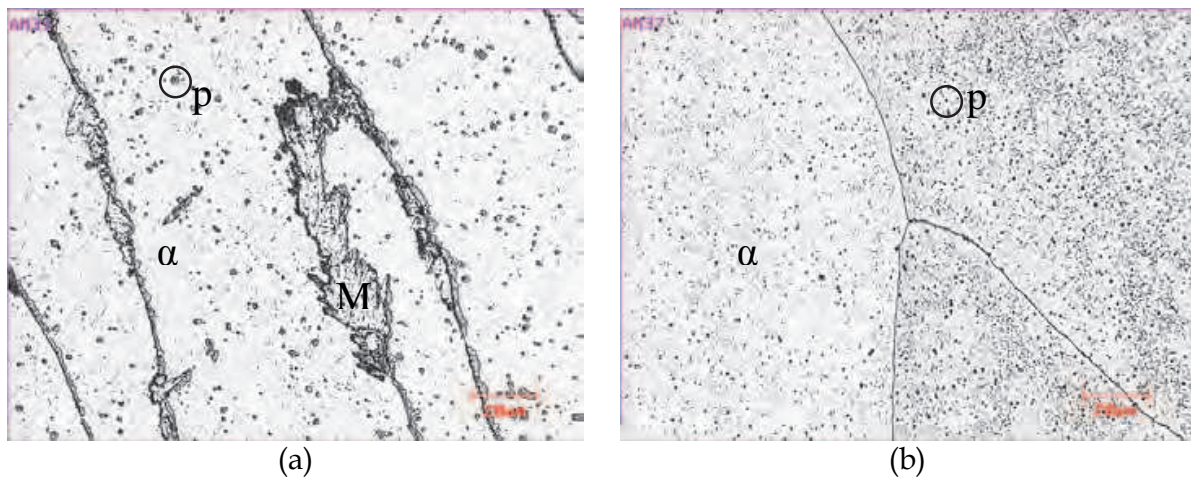


Fig. 12. Fusion zone microstructure with Ar+4%CO₂ as shielding gas for the ER430Ti wire (a) and for the ER430LNb wire (b) (" α " represents ferritic matrix, "M" martensite and "p" precipitates).

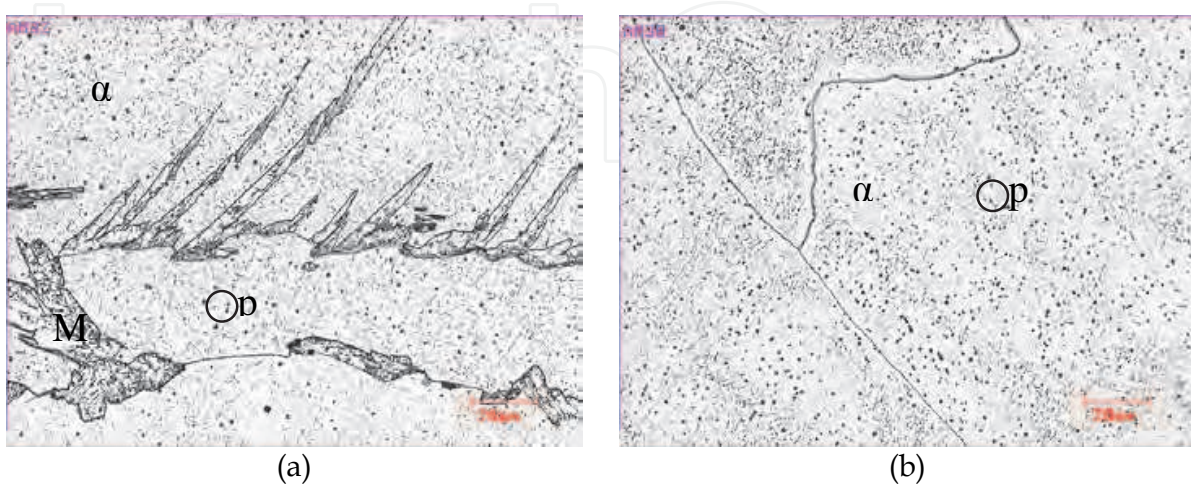


Fig. 13. Fusion zone microstructure with Ar+8%CO₂ as shielding gas for the ER430Ti wire (a) and for the ER430LNb wire (b) (" α " ferritic matrix, "M" martensite and "p" precipitates).

3.3 Weld microstructure in the square butt joints

Based on the base and filler metals chemical compositions (Table 1 and 2, respectively) and in a dilution level of 39% (mean level for all shielding gases used), the microstructures and chemical compositions were estimated through Schaeffler diagrams for the case of weld beads produced using the ER430Ti wire (Figure 14 and 15).

As seen in Figure 14, the ER430Ti filler metal is located in the ferrite-martensite region, whilst the base metal falls in the ferritic region. The weld bead is located on the border between the ferritic and ferritic-martensitic regions, that is, carbon additions might lead to martensite formation in the fusion zone. Also from the diagram, the weld beads are estimated to have 0.070% of carbon, 0.79% of silicon, 0.46% manganese, 17.29% of chromium, 0.33% of nickel and 0.07% of niobium.

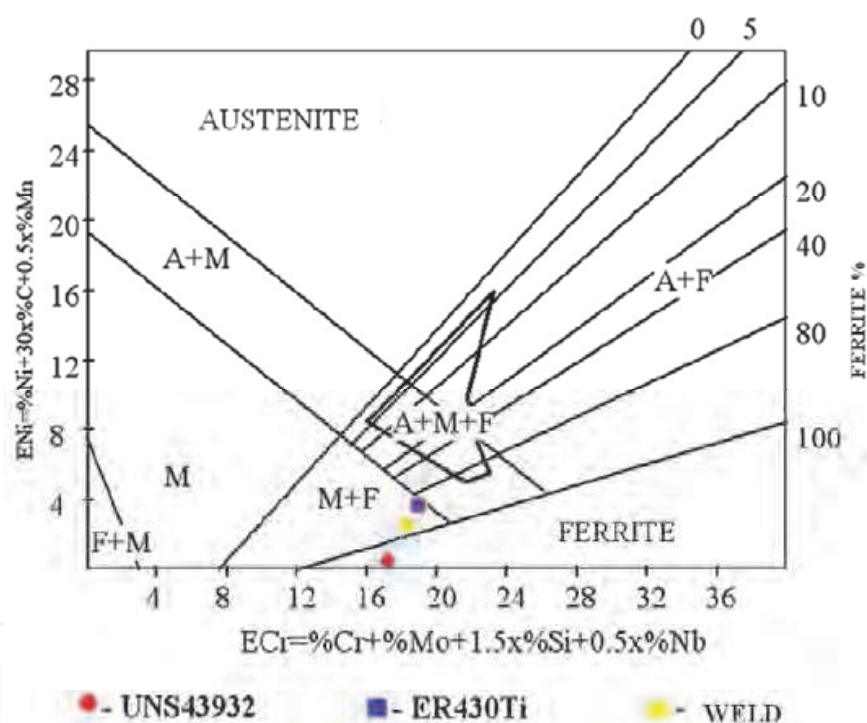


Fig. 14. Schaeffler diagram applied to the samples produced with the ER430Ti wire.

Applying the Schaeffler diagram methodology also to the samples welded with the ER430LNb wire (Figure 15), just ferritic microstructure was estimated to take place in the fusion zone. Concerning the chemical composition, the weld beads in this case are expected to have 0.023% of carbon, 0.12% of silicon, 0.35% of manganese, 17.49% of chromium, 0.38% of nickel and 0.37% of niobium.

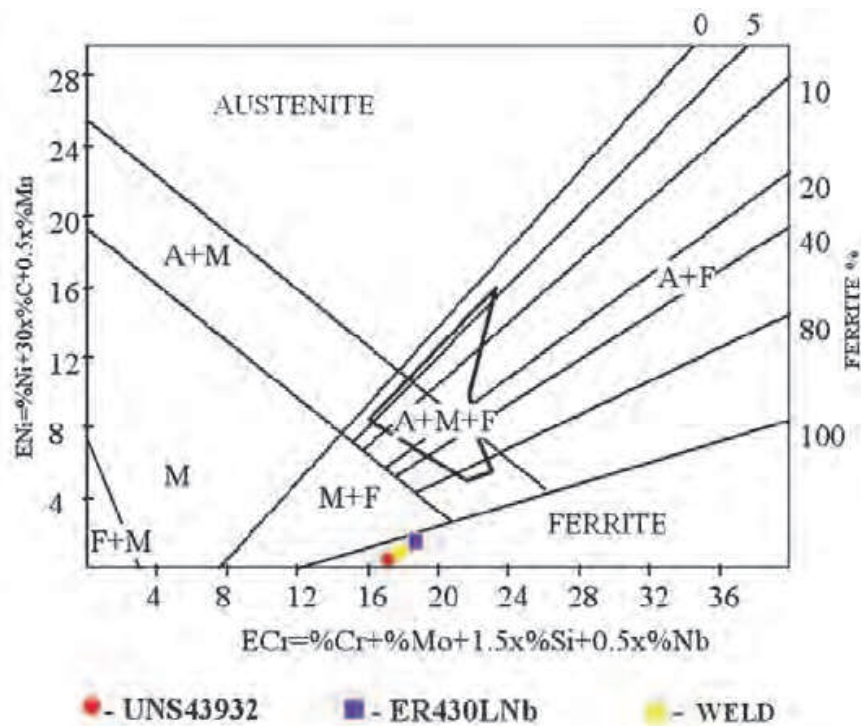


Fig. 15. Schaeffler diagram applied to the samples produced with the ER430LNb wire.

Figures 16 to 19 present the fusion zone microstructure produced by the ER430Ti and ER430LNb wires for, respectively, Ar, Ar+2%O₂, Ar+4%CO₂ and Ar+8%CO₂ as shielding gases.

In the ER430Ti wire case (Figures 16(a) a 19 (a)), a ferritic matrix with titanium precipitates was observed in all grains, structure also observed by Madeira (2007) using SEM. Throughout the images it is possible to notice the increase in the amount of precipitates all around as the CO₂ content in the gas was raised. This fact is due to the increase in the presence of carbon in the fusion zone. It is worth saying that large carbon amounts can also form chromium precipitates, which decrease the corrosion resistance of the weld beads.

The estimations carried out by Schaeffler diagrams, in which titanium is not taking into account, showed the presence of ferrite and martensite along the grain boundaries in the microstructures. However, this was not the case of the weld beads produced using up to 8% of CO₂. This fact shows that titanium, up to this level of CO₂, was successful as a stabilizing element.

In the ER430LNb wire case (Figures 16 (b) a 19 (b)), a ferritic matrix with probably Nb precipitates formed in all grains. Despite it was not measured, an increase in the number of precipitates is visually verified as the CO₂ content in the gas was raised, but not as remarkable as for the ER430Ti wire case. The increase in the presence of C in the fusion zone is likely the reason for the increasing number of precipitates in the ER430LNb case as well.

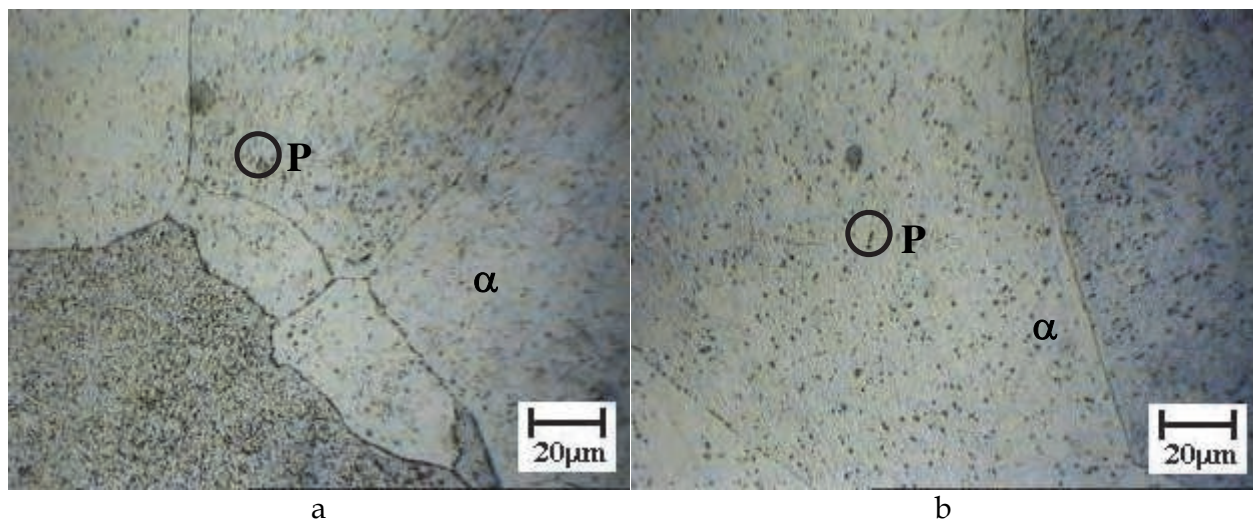


Fig. 16. Fusion zone produced with Ar as shielding gas and with the ER430Ti wire (a) and with the ER430LNb wire (b) (α) ferritic matrix, (P) titanium or niobium precipitates).

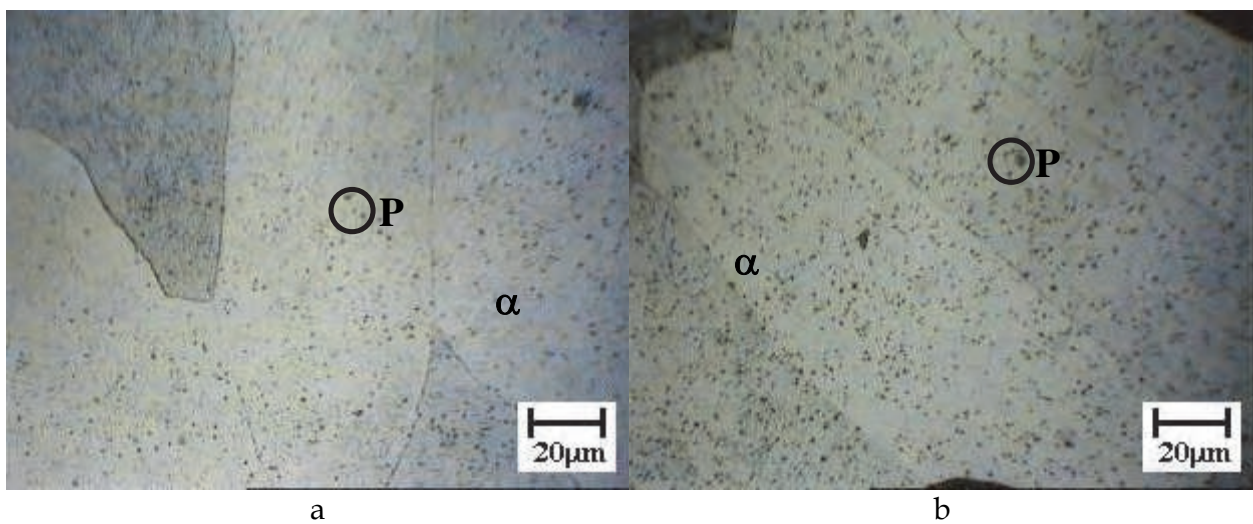


Fig. 17. Fusion zone produced with Ar+2%O₂ as shielding gas and with the ER430Ti wire (a) and with the ER430LNb wire (b) (α) ferritic matrix, (P) titanium or niobium precipitates).

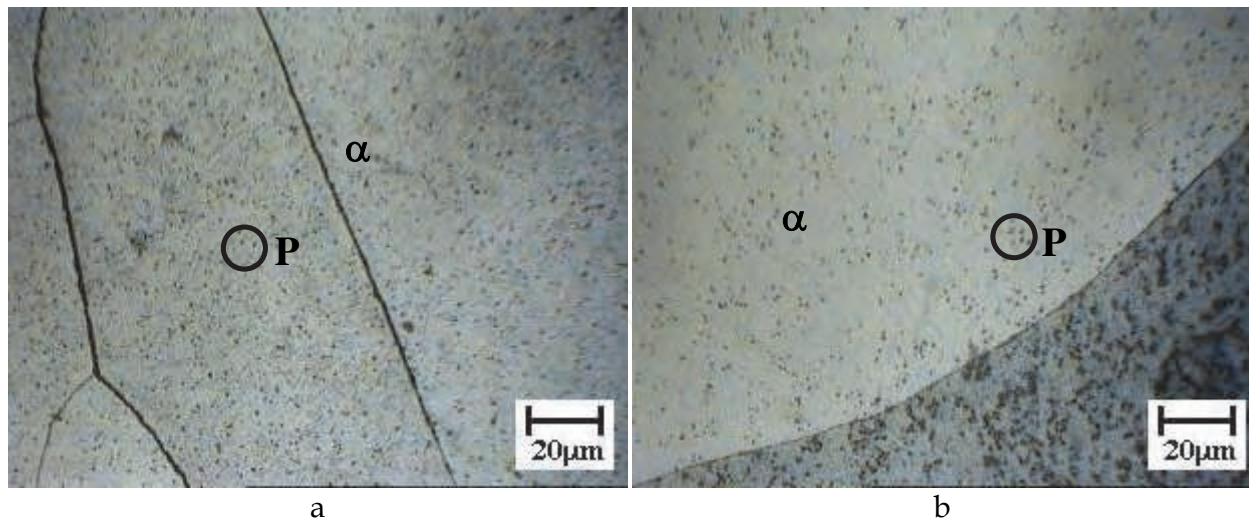


Fig. 18. Fusion zone produced with Ar+4%CO₂ as shielding gas and with the ER430Ti wire (a) and with the ER430LNb wire (b) ((α) ferritic matrix, (P) titanium or niobium precipitates).

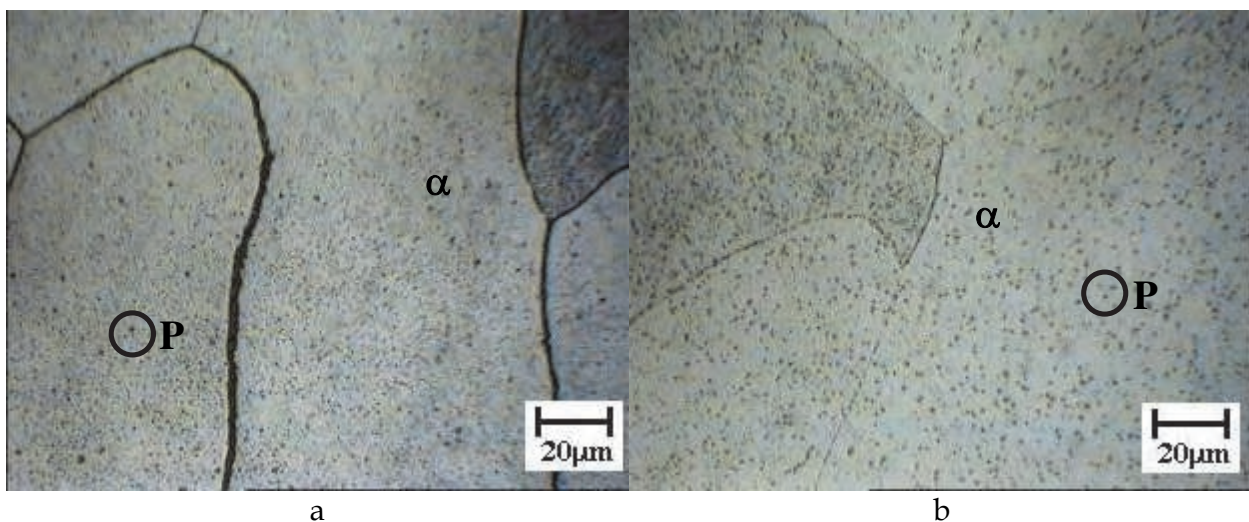


Fig. 19. Fusion zone produced with Ar+8%CO₂ as shielding gas and with the ER430Ti wire (a) and with the ER430LNb wire (b) ((α) ferritic matrix, (P) titanium or niobium precipitates).

As martensite was not observed along the grain boundaries with shielding gases with up to 8% of CO₂ in the weld beads produced in the square butt joints (with dilution), but it was found in the weld beads with dilution from 4% of CO₂ and using the ER430Ti wire, an extra shielding gas containing 25% of CO₂ was assessed for both wires.

As showed in Figure 20 (a), for the ER430Ti case, besides the formation of ferritic matrix and precipitates, there is also martensite formed along the grain boundaries when 25% of CO₂ is used in the shielding gas. In this case, the titanium present in the wire was unable to cause an adequate stabilization and the free carbon leads to transformation of austenite into martensite during the weld bead cooling. For the ER430LNb wire case (Figure 20 (b)), there was not martensite present in the weld beads even with the use of such level of CO₂. In this case, the niobium in this wire was able to stabilize the carbon for all the shielding gases.

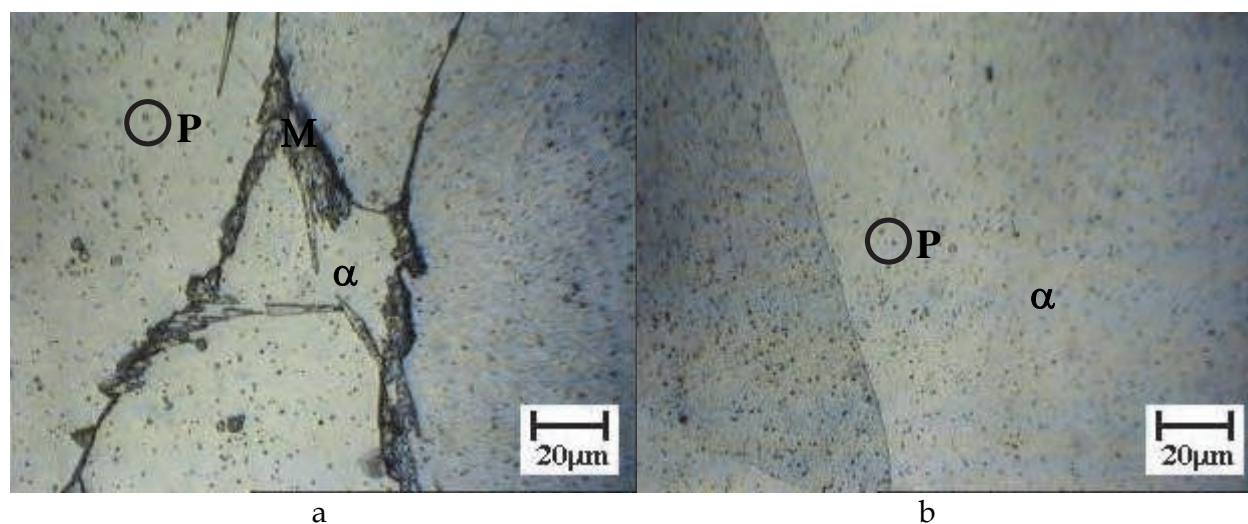


Fig. 20. Fusion zone produced with Ar+25%CO₂ as shielding gas and with the ER430Ti wire (a) and with the ER430LNb wire (b) ((α) ferritic matrix, (P) titanium or niobium precipitates, (M) martensite).

3.4 Welded joints microhardness

Table 4 presents the microhardness values measured in the ferritic matrix for the ER430Ti and ER430LNb wires. Table 5 shows the microhardness values measured in the martensite formations in the weld beads produced with the ER430Ti wire and with Ar+25%CO₂ as the shielding gas.

Wire	Shielding gas	Microhardness (HV _{2,5})	
		Mean value	Standard deviation
ER430Ti	Ar	180.3	1.5
	Ar+2%O ₂	172.0	10.6
	Ar+4%CO ₂	187.7	4.7
	Ar+8%CO ₂	208.0	4.6
	Ar+25%CO ₂	203.0	1.0
ER430LNb	Ar	163.0	2.6
	Ar+2%O ₂	173.0	1.0
	Ar+4%CO ₂	160.3	7.2
	Ar+8%CO ₂	182.0	3.6
	Ar+25%CO ₂	181.3	2.9

Table 4. Microhardness values measured in the weld beads produced with the ER430Ti and ER430LNb wires.

Wire	Shielding gas	Microhardness (HV2.5)						
		1	2	3	4	5	Mean value	Standard deviation
ER430Ti	Ar+25%CO ₂	245	269	304	304	364	292.3	20.2

Table 5. Microhardness values measured in the martensite formations in the fusion zone.

Figures 21 and 22 show graphically, for the ER430Ti wires ER430LNb respectively, the microhardness values observed in the fusion zones versus the shielding gas used. The microhardness values taken from the ferritic matrix of the weld beads produced with the ER430Ti wire and with argon and Ar+2%O₂ as shielding gases were very similar to those measured in the base metal ferritic matrix. With the addition of CO₂ in the shielding gas there was a significant rise in the microhardness levels, which was probably due to the large number of Ti precipitates present, as seen in Figures 16 to 20. With Ar+25%CO₂, martensite was formed along the grain boundaries, which is put in evidence by the elevated microhardness levels observed in this case.

Cardoso (2003) observed a microhardness value close to 350 HV_{2.5} with the use of Ar+8%CO₂. According to him, such level of hardness would cause decrease in the union toughness. As microhardness values of magnitudes close to this level were found on the martensite region in the weld beads produced with the ER430Ti wire, loss of toughness in such weld beads is also expected to take place.

The microhardness values measured in the ferritic matrix of the weld beads produced with the ER430LNb wire were very close to the values found in the base metal ferritic matrix. In general, no major variation in the microhardness levels were noticed as the shielding gas was changed in this case.

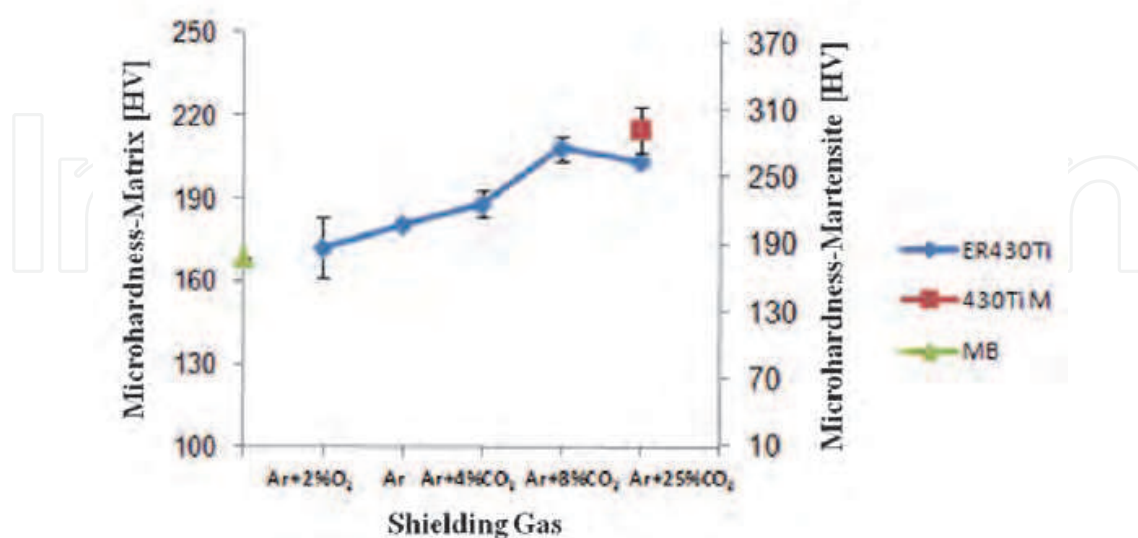


Fig. 21. Microhardness values in the fusion zone of the weld beads produced with the ER430Ti wire versus the shielding gas used.

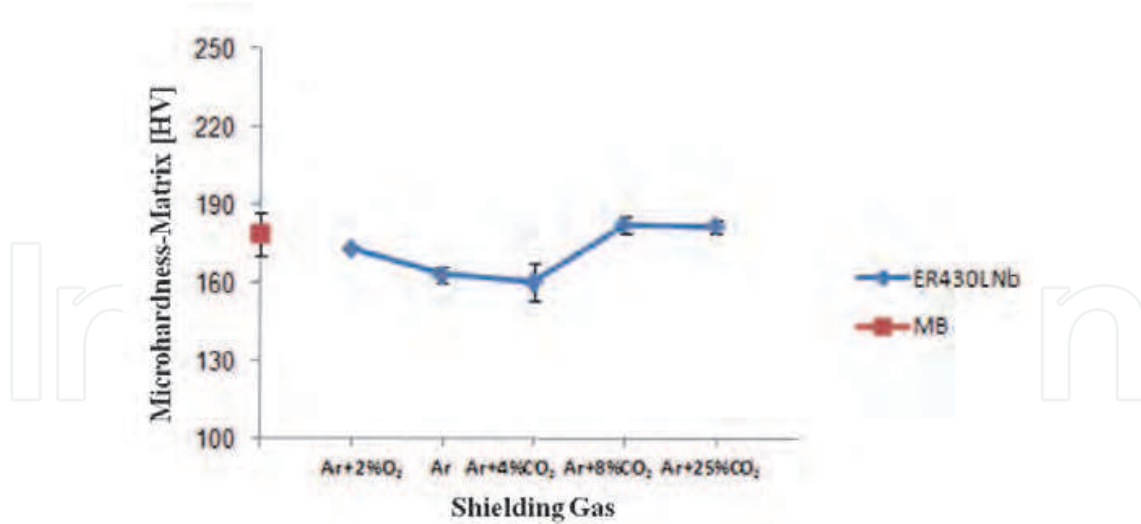


Fig. 22. Microhardness values in the fusion zone of the weld beads produced with the ER430LNb wire versus the shielding gas used.

3.5 Welded joints ductility

Figures 23 and 24 show the evolution of the loads supported by the welded samples during the stampability tests along with the aspect of the samples after the tests for, respectively, Ar+2%O₂ and Ar+25%CO₂ as the shielding gas.

For the sample welded using Ar+2%O₂ the failure (crack) of the weld bead took place along the welding direction. In contrast, for the sample welded with Ar+25%CO₂ the fracture took place transversally to the welding direction. Madeira (2007) also reported these two forms of fractures in stampability tests of welded joints. According to him, transversally cracks (failures) assure that the weld bead ductility is being evaluated.

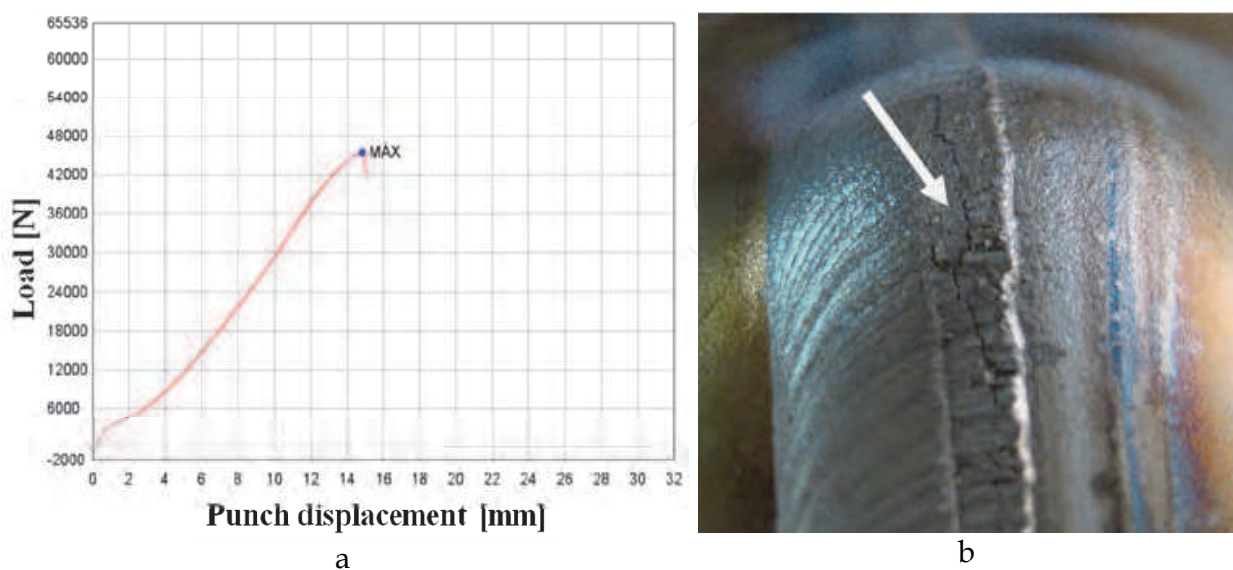


Fig. 23. Stampability test for the condition using the ER430Ti wire and Ar+2%O₂ as the shielding gas (loads supported by the sample (a) and aspect of the sample after the test (b)).

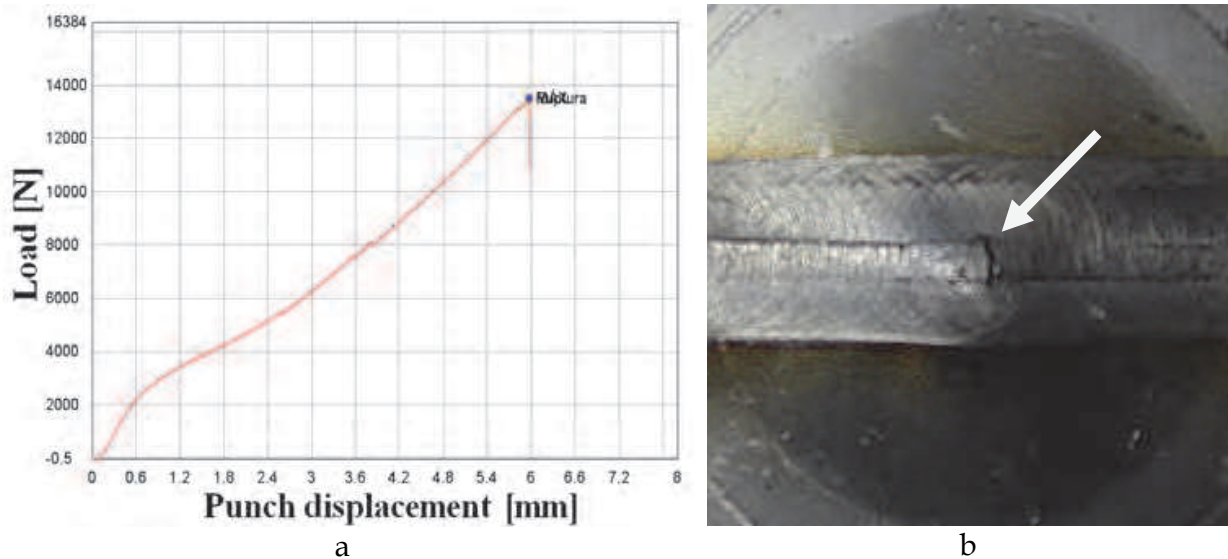


Fig. 24. Stampability test for the condition using the ER430Ti wire and Ar+25%CO₂ as the shielding gas (loads supported by the sample (a) and aspect of the sample after the test (b)).

Table 6 presents the values of the maximum loads supported by the samples and also the punch displacements and energies absorbed during the stampability tests of weld beads produced using the ER430Ti wire. Tests were carried out for loads applied both on the weld face and root.

Shielding gas	Loading side	Mean FMAX [N]	FMAX STD	Mean D 10-3 [m]	D STD.	E [J]	E STD
Ar	Root	41636	5370	13,5	1,9	265	85
Ar+2%O ₂	Face	27883	13879	9,7	3,9	139	117
Ar+2%O ₂	Root	26070	2448	9,9	0,7	149	35
Ar+4%CO ₂	Face	22371	8412	8,1	2,3	98	42
Ar+4%CO ₂	Root	23538	2662	8,7	0,9	92	21
Ar+8%CO ₂	Face	18951	8370	7,2	2,2	66	44
Ar+8%CO ₂	Root	29584	0	10	0,0	131	0
Ar+25%CO ₂	Face	11326	3054	5,2	1,0	31	12
Ar+25%CO ₂	Root	4909	375	2,4	0,3	7	2

FMAX = mean maximum load; D = punch displacement; E = energy absorbed; STD = standard deviations

Table 6. Values of the maximum loads supported by the samples, punch displacements and energies absorbed during the stampability tests of weld beads produced using the ER430Ti wire.

Figures 25 to 27 graphically present the trends found in the stampability tests of the samples welded with the ER430Ti wire. As seen, in general the evolution of the parameters analyzed was similar to each other and always lower than the value found for the base metal. This fact was also observed by Hunter & Eagar (1980), Sawhill & Bond (1976) and Redmond (1977). There was also a decrease in the values of the maximum loads supported by the samples, punch displacements and energies absorbed during the stampability tests as the CO₂ percentage in the shielding gas was increased, which was more evident for 25% of CO₂. When the CO₂ content in the shielding gas was increased in the welded samples produced with the ER430Ti wire there was an increase in the microhardness levels (Figure 21), decrease in the grain size and increase in the number of precipitates (Figures 16 to 20). For the case of 25% of CO₂ in particular, there was formation of martensite. All these factors justify the decrease in the levels of the stampability parameters assessed and so the decrease in the welded joints ductility.

Madeira & Modenesi (2010) also observed falls in the ductility of welded joints when they used the ER430Ti wire with an active shielding gas. They referred to the content of carbon, nitrogen and titanium in the fusion zone as the responsible for the fragilization of the joints as these elements form precipitates along the grains. However, the results found here are opposite to those presented by Washko & Grubb (1991), who state that the presence of titanium in the weld beads minimize the loss of ductility. Considering the high presence of carbon in the ER430Ti wire (Table 1) and the high levels of carbon getting into the fusion zone from the CO₂ added to the shielding gas, the titanium present in this filler metal does not offer adequate stabilization.

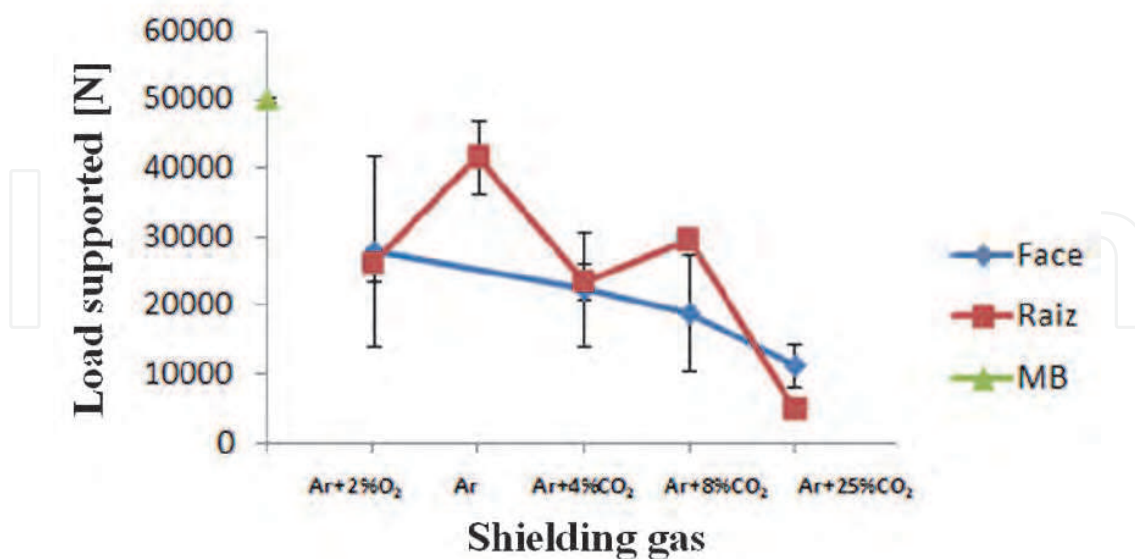


Fig. 25. Maximum loads supported by the samples produced with the ER430Ti wire versus the shielding gas used.

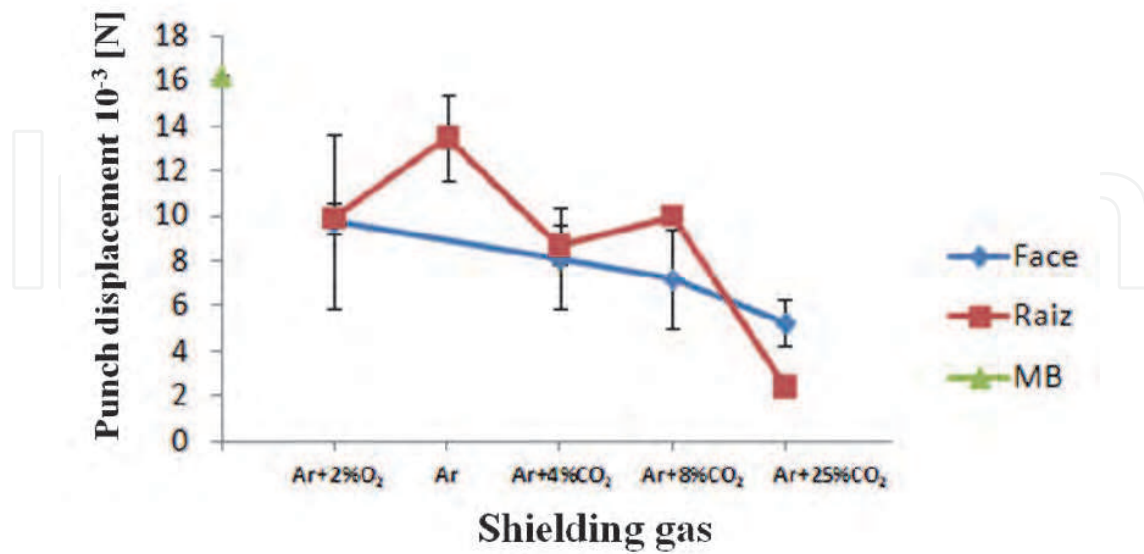


Fig. 26. Punch displacement in the samples produced with the ER430Ti wire versus the shielding gas used.

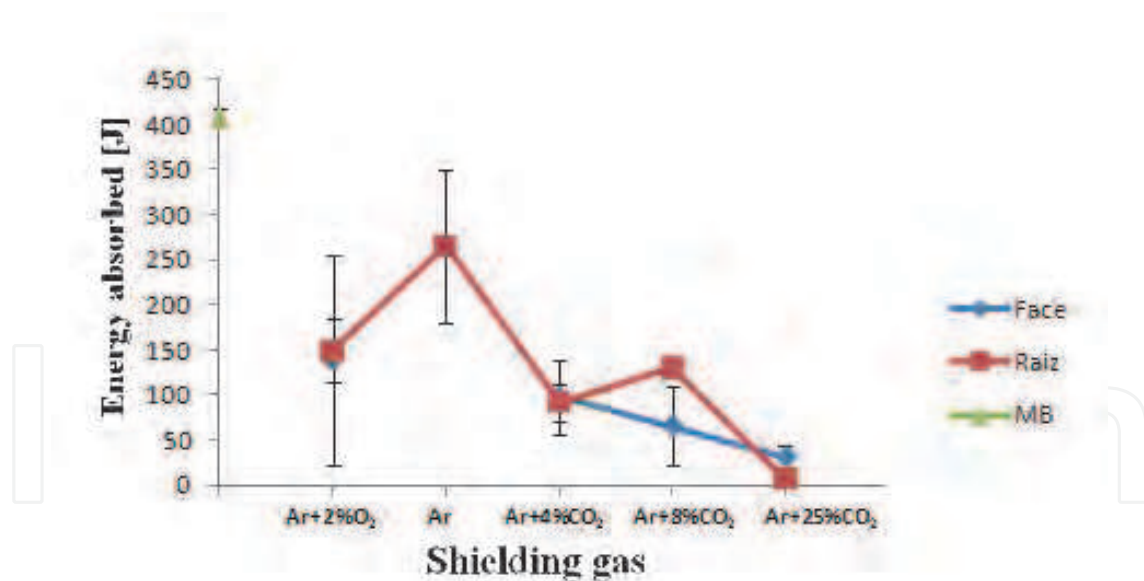


Fig. 27. Energy absorbed by the samples produced with the ER430Ti wire versus the shielding gas used.

Table 7 presents the values of the maximum loads supported by the samples and also the punch displacements and energies absorbed during the stampability tests of weld beads produced using the ER430LNb wire. As for the ER430Ti wire case, the tests were carried out for loads applied both on the face and root of the weld beads.

Shielding gas	Loading side	Mean FMAX [N]	FMAX STD	Mean D 10-3 [m]	D STD.	E [J]	E STD
Ar	Face	40065	11277	13.1	3.1	261	131
Ar	Root	17381	1514	7.0	0.6	56	10
Ar+2%O ₂	Face	32792	10751	11.3	2.8	181	101
Ar+2%O ₂	Root	24101	10286	8.9	3.2	108	84
Ar+4%CO ₂	Face	36152	1413	11.7	0.6	184	18
Ar+4%CO ₂	Root	32158	20096	11.2	5.4	210	211
Ar+8%CO ₂	Root	21440	14611	8.8	3.0	102	85
Ar+25%CO ₂	Face	34068	0	11.2	0	236	0
Ar+25%CO ₂	Root	16845	8546	7.0	2.6	76	32

FMAX = mean maximum load; D = punch displacement; E = energy absorbed; STD = standard deviations

Table 7. Values of the maximum loads supported by the samples, punch displacements and energies absorbed during the stampability tests of weld beads produced using the ER430LNb wire.

Figures 25 to 27 graphically present the trends found in the stampability tests of the samples welded with the ER430LNb wire. With this wire no significant variations in the parameters assessed was recorded. The dispersion in the results for each shielding gas might have occurred due to possible fragilization in the weld beads that was not perceived during the visual analyses of the samples.

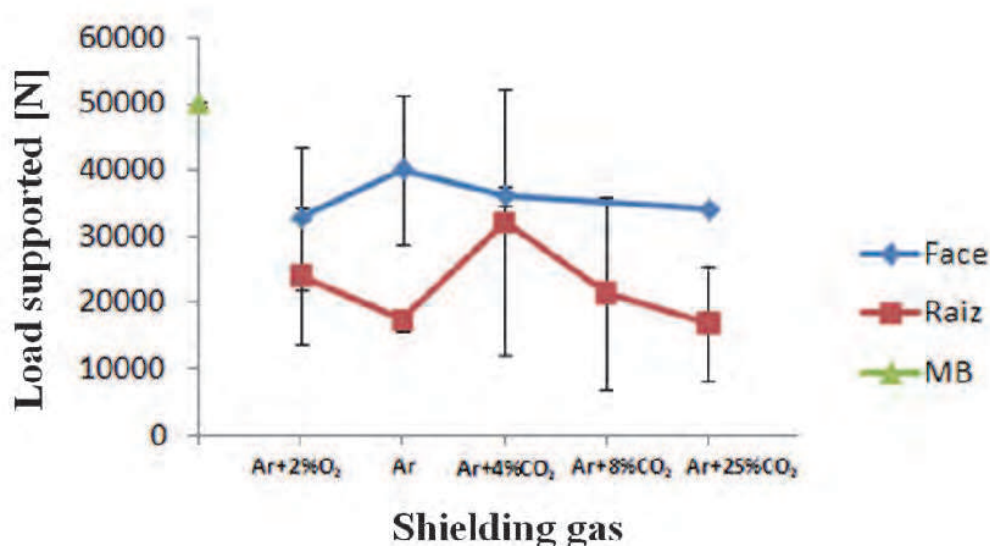


Fig. 28. Maximum loads supported by the samples produced with the ER430LNb wire versus the shielding gas used.

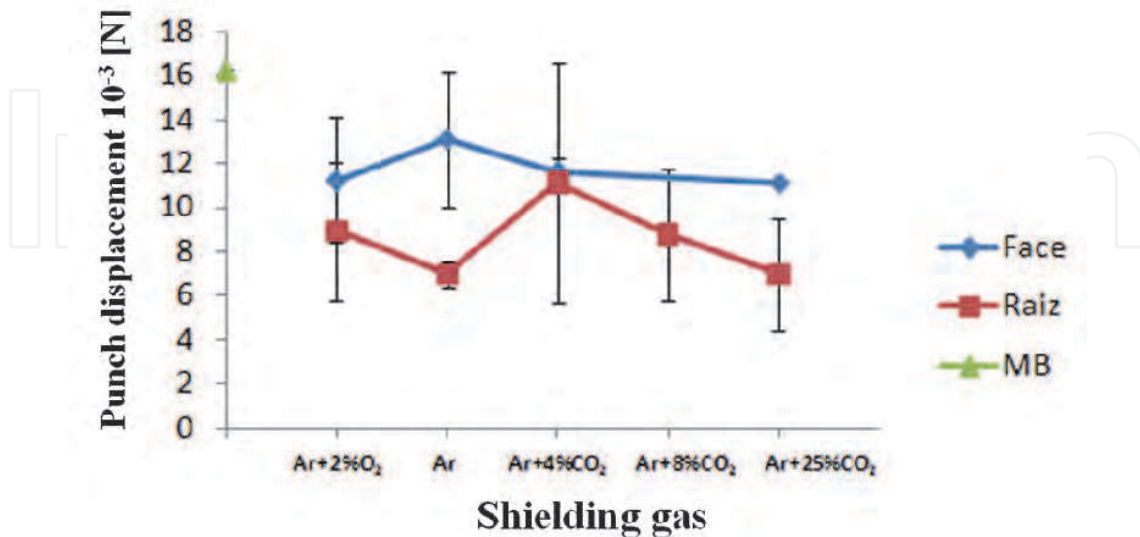


Fig. 29. Punch displacement in the samples produced with the ER430LNb wire versus the shielding gas used.

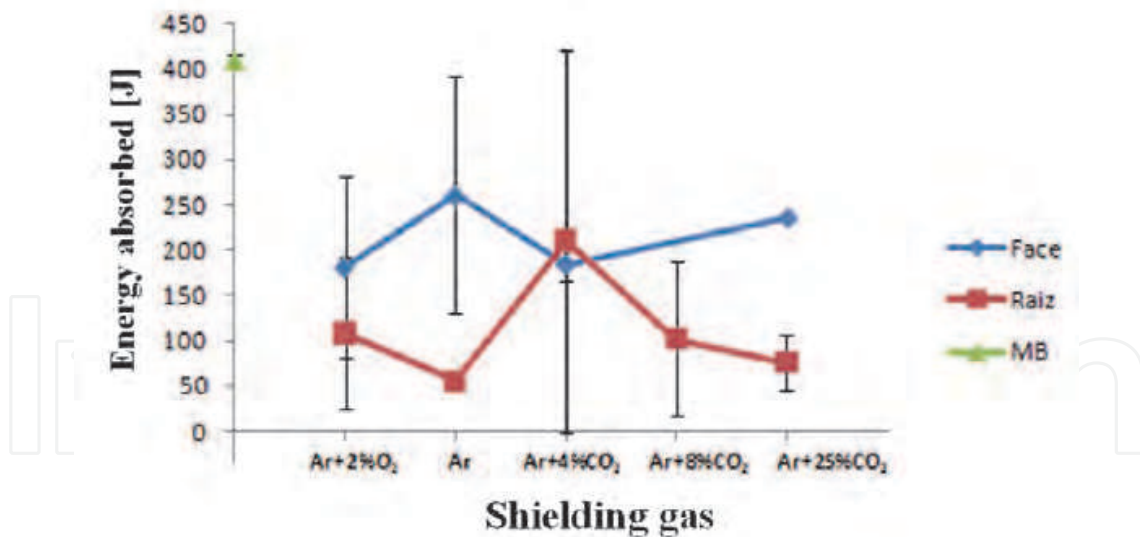


Fig. 30. Energy absorbed by the samples produced with the ER430LNb wire versus the shielding gas used.

Taking into account the results of the stampability tests, it is possible to consider that the increase in the CO₂ content in the shielding gas decreases the ductility of the welded joints if the ER430Ti wire is used. If the ER430LNb wire is utilized instead, it performs a better stabilization of the C present and the result is that no significant variations are recorded for the welded joints ductility even with the high levels of CO₂ added to the shielding gas.

4. Conclusions

Considering the conditions and results presented in this chapter, the conclusions can be summarized as:

- For the ER430Ti and ER430LNb wires, the addition of CO₂ in the shielding gas promotes an increase in the quantity of carbon and a decrease in the amount of manganese, silicon, and also in the stabilizing elements (titanium and niobium, respectively);
- In the welded layers (without dilution), the titanium present in the ER430Ti wire was insufficient to avoid the formation of martensite in the fusion zone with the use of levels of CO₂ higher than 4%. Also without dilution in the welded joint, but using the ER430LNb wire, martensite did not form with shielding gases with up to 8% of CO₂;
- In the weld beads produced in square butt joints using the ER430Ti wire, martensite was only noticed for the weld beads produced with 25% of CO₂. Also in square butt joints but using the with ER430LNb, the stabilization was effective and no martensite formation was verified even for such level of CO₂;
- An increase in hardness and therefore a fall in the ductility of the welded joints took place for the ER430Ti wire. This fact was not recorded for the weld beads produced with the ER430LNb wire.
- Therefore, the ER430LNb was the best wire utilized for the selected conditions.

In face of the conclusions, this manuscript shows the importance of correct stabilization of a filler metal in welding. Besides that, the shielding gas may play a decisive role in the ductility of welded joints, so as in the microstructures formed. As verified, it is possible to utilize ferritic stainless steel filler metals in welding approaches for ferritic stainless steel components by using low-cost shielding gases and at the same time preserve the joint properties. This shows that the tendency of using austenitic stainless steel filler metals with high-cost shielding gases for ferritic stainless steel welded components might be equivocated.

5. Acknowledgments

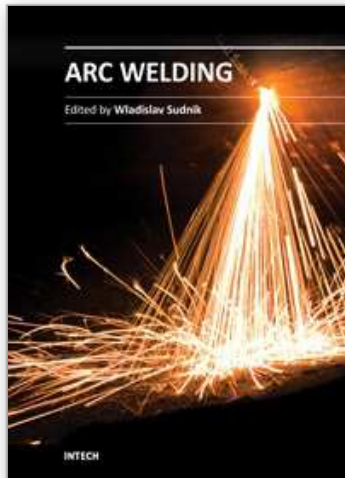
The authors express their gratitude to CNPq, CAPES, Fapemig, Fapergs, Federal University of Rio Grande, Federal University of Uberlândia and LAPROSOLDA/UFU for the infrastructure and, especially, to ACELORMITTAL and WhiteMartins for providing the materials used in the experiments.

6. References

- Alves, H.J.B, Carvalho, J.N., Aquino, M.V., Mantel, M.J. (2002). Development of ferritic stainless steels for automotive exhaust systems. *Proceedings of 4th Stainless Steel Science and Market Congress*, Paris, France, June 2002.
- Balmforth, M. C.; Lippold, J. C. (2000) A New Ferritic-Martensitic Stainless Steel Constitution Diagram. *Welding Journal*, Vol. 79, n. 12 (Dec. 2000), pp. 339s-345s, ISSN 0043-2296.
- Cardoso, R. L.; Prado, E. M.; Okimoto, P. C.; Paredes, R. S. C., Procopiak, L. A. (2003). Avaliação da Influência de Gases Proteção Contendo Diferentes Teores de CO₂ nas Características dos Revestimentos Soldados Visando o Reparo de Turbinas

- Erodidas por Cavitação. *Soldagem & Inspeção*, Ano 8, n. 2, (April-Jun. 2003), pp. 68-74, ISSN 0104-9224.
- Chae, H. B., Kim, C. H., Kim, J. H., Rhee, s. (2008). The effect of shielding gas composition in CO₂ laser-gas metal arc hybrid welding. *Proc. IMechE, Part B: J. Engineering Manufacture*, Vol. 222 (2008), pp. 1315-1324, ISSN 0954-4054.
- Durgutlu, A. (2004). Experimental Investigation of the Effect of Hydrogen in Argon as a Shielding Gas on TIG Welding of Austenitic Stainless Steel, *Materials & Design*, Vol. 25, Issue 1 (Feb. 2004), pp.19-23, ISSN 0264-1275.
- Faria, R. A. (2006). *Efeito dos elementos Ti e Nb no comportamento em fadiga em aços inoxidáveis ferríticos utilizados nos sistemas de exaustão de veículos automotores*, 245 f., (PhD Thesis) Universidade Federal de Ouro Preto, Ouro Preto, MG, Brazil..
- Ferreira Filho, D. ; Ferraresi, V A ; Scotti, A. (2010). Shielding gas influence on the ferritic stainless steel weldability. *Proceedings of the Institution of Mechanical Engineers. Part B, Journal of Engineering Manufacture*, v. 224, (2010), pp. 951-961, ISSN 0954-4054.
- Filho, Demostenes Ferreira ; Ferraresi, Valtair Antonio. (2010). The influence of gas shielding composition and contact tip to work distance in short circuit metal transfer of ferritic stainless steel. *Welding International*, v. 24, pp. 206-213, ISSN 0950-7116.
- Ferreira Filho, D.; Ferraresi, V. A. . Influência do tipo de gás de proteção e da distância bico de contato-peça na transferência metálica do modo curto-circuito do aço inoxidável ferrítico. *Soldagem & Inspeção*, v. 13, n. 3, (Jul. 2010), pp. 173-180, ISSN 0104-9224.
- Gülenç, B., Develi, K., Kahraman, N. , Durgutlu, A. (2005). Experimental Study of the Effect of Hydrogen in Argon as a Shielding Gas in MIG Welding of Austenitic Stainless Steel, *International Journal of Hydrogen Energy*, Vol. 30, Issues 13-14, (October-November 2005), pp. 1475-1481, ISSN 0360-3199.
- Hiramatsu, N. (2001). *Niobium in ferritic and martensitic stainless steels*. Proceedings of the International Symposium Niobium, Orlando, Florida, USA, 2001.
- Hunter, G. B., Eagar, T. W., (1980) Ductility of stabilized ferritic stainless steel welds. *Metallurgical Transactions A*, v. 11 A (Feb 1980), p. 213-218.
- Inui, K., Noda, T., Shimizu, T. (2003). *Development of the Ferritic Stainless Steel Welding Wire Providing Fine Grain Microstructure Weld Metal for the Components of Automotive Exhaust System*, Proceedings of SAE International 2003, World Congress and Exhibition, Detroit USA, 2003.
- Lee, C-H., Chang, K-H. And Lee, C-Y. (2008). Comparative study of welding residual stresses in carbon and stainless steel butt welds. *Proc. IMechE, Part B: J. Engineering Manufacture*, 222(B12) (2008), pp. 1685-1694, ISSN 0954-4054.
- Liao, M. T., Chen, W. J. (1998). The effect of shielding-gas compositions on the microstructure and mechanical properties of stainless steel weldments, *Materials Chemistry and Physics*, Vol. 55 (1998), p. 145-155, ISSN 0254-0584.
- Lundqvist, B. (1980). *Aspects of Gas-Metal Arc Welding of Stainless Steels*, Proceedings of Swedish. Sandvik AB, Sandviken, Sweden, 1980.
- Madeira, R. P., Modenesi, P. J. (2007). *Estudo dos arames ferríticos 430Ti e 430LNb para a aplicação na parte fria de sistemas de exaustão automotivos*, Proceedings of XXXIII CONSOLDA, Caxias do Sul-RS Brasil, 2007.
- Madeira, R. P., Modenesi, P. J. (2010). Utilização do Ensaio Erichsen para a Avaliação do Desempenho de Juntas Soldadas, *Soldagem & Inspeção*, v. 15, n. 1 (Jan/Mar 2010), p. 022-030, ISSN 0104-9224.

- Madeira, R. P. (2007). *Influência do Uso de Arames Inoxidáveis Ferríticos nas Características da Zona Fundida de um Aço Inoxidável Ferrítico com 17% de Cromo Bi-estabilizado*, 151 f., (Master's Dissertation). Universidade Federal de Minas Gerais, Belo Horizonte, MG, Brazil.
- Modenesi, P. J. (2001). *Soldabilidade dos Aços Inoxidáveis*, Vol. 1, SENAI, ISBN 85-88746-02-6, Osasco, SP, Brazil.
- Reddy, G. M.; Mohandas, T. (2001). Explorative studies on grain refinement of ferritic stainless steel welds. *Journal of Materials Science Letters*, Vol. 20, pp. 721-723, ISSN 0261-8028.
- Redmond, J. D. (1977). Climax Molybdenum Co. *Report RP.*, (Sept. 1977), p. 33-76, ISSN 0034-4885.
- Renaudot, N.; Santacreu, P. O.; Ragot, J.; Moiron, J. L.; Cozar, R.; Pédarré, P.; Bruyère, A. (2000), *430LNb - A new ferritic wire for automotive exhaust applications*. Proceedings of SAE 2000 World Congress, Detroit, MI, USA, March 2000.
- Resende, A. (2007) *Mapeamento paramétrico da soldagem GMAW com arames de aço inoxidável ferrítico e austenítico*, 126 f, (Master's Dissertation). Universidade Federal de Minas Gerais, Belo Horizonte, MG, Brazil.
- Sawhill, J. M.; Bond, A. P. (1976). Ductility and Toughness of Stainless Steel Welds, *Welding Journal*. v. 55, n. 2, p.33s. 1976, ISSN 0043-2296.
- Schwarz; B.; Tessin, F. (2003). ESAB high-alloyed welding consumables for ferritic stainless steel exhaust systems, *Svetsaren The Esab Welding and Cutting Journal*, V. 58 N.2, p. 27, 2003.
- Sekita, T., Kaneto, S., Hasuno, S., Sato, A., Ogawa, T., Ogura, K. (2004). Materials and Technologies for Automotive Use, *JFE GIHO* N. 2 (Nov. 2004), p. 1-16, ISSN 1348-0669.
- Stenbacka, N., Persson, K (1992). Shielding gases for gas-metal arc welding of stainless steels, *AGA AB Inovation*, Suécia, 1992.
- Strassburg F. W., *Schweissen nichtrostender Stähle*, DVS Band 67, DCS GmbH, Dusseldorf, FRG, 1976.
- Tusek, J., Suban, M. (2000). Experimental Research of the Effect of Hydrogen in Argon as a Shielding Gas in Arc Welding of High-Alloy Stainless Steel, *International Journal of Hydrogen Energy*, Vol. 25, Issue 4 (April 2000), pp. 369-376 ISSN 0360-3199.
- Wang, H. R., Wang, W. (2008). Precipitation of complex carbonitrides in a Nb-Ti microalloyed plate steel, *Journal of Material Science*, vol. 44, issue 2 (2008), pp. 591-600, ISSN 0022-2461.
- Washko, S. D.; Grubb, J. F. (1991). *The Effect of Niobium and Titanium Dual Stabilization on the Weldability of 11% Chromium Ferritic Stainless Steels*, Proceedings of International Conference on Stainless Steels, Chiba, ISIJ, 1991.
- Yasuda, K.; Jimma, T.; Onzawa, T. (1984). Formability of butt welded Stainless Steel Thin Sheet. *Quarterly Journal of the Japan Welding Society*, v.2, n.3, p. 161-166, ISSN 02884771.



Arc Welding

Edited by Prof. Wladislav Sudnik

ISBN 978-953-307-642-3

Hard cover, 320 pages

Publisher InTech

Published online 16, December, 2011

Published in print edition December, 2011

Ever since the invention of arc technology in 1870s and its early use for welding lead during the manufacture of lead-acid batteries, advances in arc welding throughout the twentieth and twenty-first centuries have seen this form of processing applied to a range of industries and progress to become one of the most effective techniques in metals and alloys joining. The objective of this book is to introduce relatively established methodologies and techniques which have been studied, developed and applied in industries or researches. State-of-the-art development aimed at improving technologies will be presented covering topics such as weldability, technology, automation, modelling, and measurement. This book also seeks to provide effective solutions to various applications for engineers and researchers who are interested in arc material processing. This book is divided into 4 independent sections corresponding to recent advances in this field.

How to reference

In order to correctly reference this scholarly work, feel free to copy and paste the following:

Demostenes Ferreira Filho, Ruham Pablo Reis and Valtair Antonio Ferraresi (2011). Evaluation of the Shielding Gas Influence on the Weldability of Ferritic Stainless Steel, Arc Welding, Prof. Wladislav Sudnik (Ed.), ISBN: 978-953-307-642-3, InTech, Available from: <http://www.intechopen.com/books/arc-welding/evaluation-of-the-shielding-gas-influence-on-the-weldability-of-ferritic-stainless-steel>

INTECH
open science | open minds

InTech Europe

University Campus STeP Ri
Slavka Krautzeka 83/A
51000 Rijeka, Croatia
Phone: +385 (51) 770 447
Fax: +385 (51) 686 166
www.intechopen.com

InTech China

Unit 405, Office Block, Hotel Equatorial Shanghai
No.65, Yan An Road (West), Shanghai, 200040, China
中国上海市延安西路65号上海国际贵都大饭店办公楼405单元
Phone: +86-21-62489820
Fax: +86-21-62489821

© 2011 The Author(s). Licensee IntechOpen. This is an open access article distributed under the terms of the [Creative Commons Attribution 3.0 License](#), which permits unrestricted use, distribution, and reproduction in any medium, provided the original work is properly cited.

IntechOpen

IntechOpen